December 27, 2004

Dislocation Structures and the Deformation of Materials

Marisol Koslowski, *Los Alamos National Laboratory*
Richard Alan Lesar, *Los Alamos National Laboratory*
Robb Thomson, *Los Alamos National Laboratory*

Dislocation Structures and the Deformation of Materials

Marisol Koslowski,* Richard LeSar, and Robb Thomson
Theoretical Division, Los Alamos National Laboratory, Los Alamos, NM 87545, USA
(Received 22 September 2004; published 27 December 2004)

We present results from phase-field simulations of a two-dimensional model of dislocation microstructure development under increasing strain that incorporates the effects of the full, three-dimensional, microstructure in an approximate way. Despite its simplicity, the model yields quantitative predictions of both the deformation properties of face-centered cubic metals as well as key descriptors of the evolving microstructure over a wide range of stress and strain. The present results have important implications for how we interpret and describe the deformation properties of fcc materials.

DOI: 10.1103/PhysRevLett.93.265503 PACS numbers: 62.20.Fe, 61.72.Bb, 89.75.Da

As materials deform under increasing strain, dislocations are generated and complex structures develop, which in turn affect the deformation properties. For example, when an fcc metal is deformed plastically at moderate temperatures under single-slip conditions, there are several generic sequential stages of deformation, with each stage characterized by coupled macroscopic stress-strain, temperature, and microstructural features [1]. Dislocations in Stage I form an open structure that does not greatly impede their motion, and the material exhibits a linear stress (τ)-strain (γ) response, characterized by a small slope ($d\tau/d\gamma \sim \mu/10\,000$, where μ is the shear modulus) [2]. At higher strains, there is a transition to another linear stage (II), with a much steeper slope ($d\tau/d\gamma \sim \mu/200$), which exhibits a random tangled dislocation structure [2]. As the deformation proceeds, a third stage (III) develops that is characterized by a decreasing hardening rate owing to temperature-driven dynamic recovery processes and the development of a partially ordered cellular dislocation structure.

Understanding the relation between dislocation structure development and response has been a fundamental challenge for dislocation theory for decades [3]. Despite numerous models and large numbers of experiments [2,4–6], including a number of recent stochastic theories [7–9], no single methodology has proven able to describe the full range of behaviors and the transitions between them [10]. In addition to the more heuristic models, there has been an increasing use of direct three-dimensional simulations of the evolving dislocation microstructures, in which the dislocations are the simulated entities and their movement is tracked during the simulation [11–14]. These simulations are computationally expensive, limiting the maximum stress and the consequent dislocation density in the calculation. Since realistic direct simulations of the regimes of interest are not yet feasible, our goal is to identify the essential physics to be used as the basis of a two-dimensional model simulation. By comparing the predictions of this model against known, experimentally determined behavior, we can assess the validity of the model and draw inferences about what it says about the fundamental physical mechanisms in deformation.

Our model is based on the observation that the dominant motion of dislocations is in their slip plane. While movement of a dislocation off its slip plane (cross slip) is certainly possible, here we will ignore that motion. We thus consider dislocations in one slip plane (i.e., two dimensions) and model the three dimensionality by considering dislocations on other slip systems (the *forest* dislocations) that cross the simulation plane as point obstacles that alter motion within the plane, ignoring all other interactions. We employ a two-dimensional phase-field model of dislocations [15,16] to describe the evolution of dislocation structures in the slip plane. The dislocation ensemble is represented by means of an integer-valued scalar phase field, ξ, the value of which represents the extent of slip on units of the Burgers vector at a point [15]. The location of a dislocation line is associated with integer jumps in the value of the scalar field. We take the slip plane to be (x_1, x_2) with the Burgers vector, $\mathbf{b}$, in the x_1 direction. Under these conditions the energy can be written as:

$$E[\xi] = \int \left(\frac{\mu b^2}{4} \frac{K}{1 + Kd/2} |\hat{\xi}|^2 - \frac{b\hat{s}\,\hat{\xi}}{1 + Kd/2} \right) \frac{d^2k}{(2\pi)^2}, \quad (1)$$

where a superposed $\hat{}$ denotes the Fourier transform, s is the applied resolved shear stress, d is the interplanar distance, k_i is the vector in the Fourier transformed space, and

$$K = \frac{k_2^2}{\sqrt{k_1^2 + k_2^2}} + \frac{1}{1 - \nu} \frac{k_1^2}{\sqrt{k_1^2 + k_2^2}}, \quad (2)$$

where ν is the Poisson's ratio [15]. The first term in Eq. (1) represents the long range elastic interaction between dislocations; the second term is the work done by an external applied shear stress. In both terms the expression $1 + Kd/2$ is a core regularization factor whose effect is to smooth the integer-valued phase field and appears as a response of the core energy.

The slip system initially contains a random distribution of obstacles that represent forest dislocations. We compute the slip distribution ξ^{n+1} at time t_{n+1}, given the solution ξ^n at time t_n, based on a minimization of the incremental work function $W[\xi^{n+1}|\xi^n]$

$$\xi^{n+1} = \min_{\xi^{n+1}} W[\xi^{n+1}|\xi^n], \tag{3}$$

where

$$W[\xi^{n+1}|\xi^n] = E[\xi^{n+1}] - E[\xi^n] + \int f(\mathbf{x})|\xi^{n+1}(\mathbf{x}) - \xi^n(\mathbf{x})|d^2x. \tag{4}$$

The last term in Eq. (4) represents the energy cost associated with the passage of one dislocation over the point $\mathbf{x}$, i.e., with a transition of the form $\xi(\mathbf{x}) \rightarrow \xi(\mathbf{x}) \pm 1$. The field $f(\mathbf{x})$ acts as a pinning potential. Therefore the system described by Eq. (4) is analogous to the ones used in pinning or depinning type theories. These models have been widely used to describe earthquakes, magnetic systems plasticity in amorphous materials, and fluid invasion in porous media [17–21].

The 2D method described here can be solved in closed form [15], which makes it possible to study mesoscopic-sized dislocation ensembles. Periodic boundary conditions are employed with a simulation cell $L = 128\ \mu$m a side. In all the simulations, we use material parameters of copper, ($\mu = 48$ GPa, $\nu = 0.324$, and $|\mathbf{b}| = 2.56 \times 10^{-10}$ m). The results given below were obtained by averaging over 100 simulation runs. The macroscopic strain associated with the deformation is $\gamma = \gamma_0\langle\xi\rangle$, where $\langle\xi\rangle$ is the average of the phase field, $\gamma_0 = b/l$ is a reference slip strain, and l is the slip plane spacing. In the present simulations, l is chosen to be 100 b. The dislocation line density per unit volume is proportional to the gradient of the phase field as $\rho = \langle|\nabla\xi|\rangle/l$.

The calculation is started at zero stress and the stress is increased quasistatically in monotonic steps. We assume an initial (random) density of forest dislocations ($\rho_{\text{obs}} = 6 \times 10^9/\text{m}^2$) that is high compared to experiments [22]. This choice is necessitated by the system size and the limitation in our model that the only sources of mobile dislocations are the forest dislocations. Studies with other initial obstacle densities indicate that the basic physics is unchanged from that reported here. After yield, the average density of the obstacles, ρ_{obs}, is assumed to vary in accordance with the Taylor relationship between stress and dislocation density [2]

$$\tau = \alpha\mu b\sqrt{\rho}, \tag{5}$$

where α is an empirical parameter. In the present work, obstacles are introduced at each change of stress such that the average density of those obstacles on the plane scales as in Eq. (5) with $\alpha = 0.2$. The obstacle positions were chosen randomly within the simulation cell and the interaction strengths were chosen randomly from a distribution with a mean value of $f = \mu$b and a dispersion of $\delta f = 0.1f$ [15].

In Fig. 1, we show the computed stress-strain curve. Three regimes of deformation are clearly visible. In the first regime, I, there is an initial stage of easy glide until the system yields, at a critical stress $\tau = 0.10 \times 10^{-3}\mu$. During this regime the obstacles are impenetrable to the dislocations and the dislocations move through the open spaces between obstacles, leading to the formation of Orowan loops [15]. After the flow stress is reached, other slip systems become active and the density of forest dislocations (obstacles) is increased, as described above. We see an approximately linear regime in the stress-strain response (Stage II), characterized by a slope $d\tau/d\gamma \approx \mu/162$ that is in the range of the empirical value of $\mu/200$ found for generic fcc metals [2]. At a stress of about $\tau = 1.5 \times 10^{-3}\mu$ (72 MPa), we see the beginning of a gradual decrease in the slope, corresponding to the transition to what we identify as Stage III behavior.

We examined a number of measures of the dislocation distributions to correlate structure with response. We see from Fig. 2 that the expected Taylor relation [Eq. (5)] is satisfied in Stage II, with a value of $\alpha \approx 0.3$, close to the experimental result of about 0.26 [22]. In Fig. 1, we show the calculated values of the variance of the dislocation density $\sigma^2 = \langle\rho^2\rangle/\langle\rho\rangle^2 - 1$. We see that the variance exhibits a maximum at a stress corresponding to the transition from Stage II to III that we identified from the stress-strain curve. A similar relation between the peak in the variance and the Stage II/III transition has recently been seen experimentally [21]. The calculated peak value of σ^2 is about 2.4, in comparison with the experimental value of 2.6 at 300 K [22].

We show the calculated evolution of the deformation in Fig. 3 as a function of stress. In the top figures, we show the deformation patterns (i.e., the value of the phase field, which corresponds to the amount of slip), where the local density of dislocations can be found by taking the gradient of the deformation field. The calculated deformation along

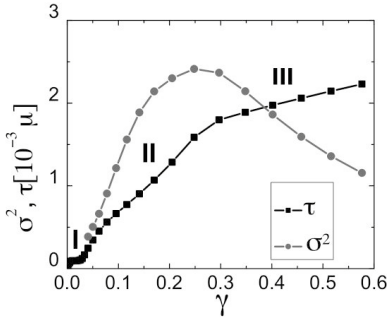

FIG. 1. Calculated strain-stress curve and the evolution of the variance of the dislocation density, as described in the text. The stress is given in units of $10^{-3}\mu$.

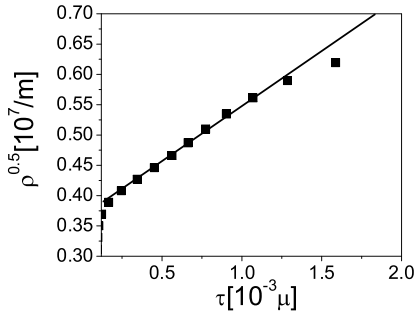

FIG. 2. Evolution of the square root of the dislocation density with the applied shear stress with a fitted relation $\tau \sim \mu b\sqrt{\rho}$.

a horizontal line at the center of the simulation cell is shown in the bottom figures, which are plotted on the same scale relative to each other and are centered at the average value of the slip for each stress state. Cell walls can be identified as vertical lines of dense regions of dislocations separating regions of lower, relatively constant density (upper figures) and manifest themselves as sharp changes in slope in the deformation plots (bottom figures).

Figure 3(a) was calculated at a stress corresponding to the end of Stage I in Fig. 1. Dislocation loops bow through the open spaces between obstacles and there is no discernible organization of the dislocations. The total deformation shows little variation across the simulation cell (bottom figure). In Fig. 3(b), we see the beginning of the development of a cell structure, as indicated by increases in local dislocation density in the microstructure and shallow regions of constant deformation separated by regions of higher dislocation content (bottom figure). Other slip systems have become active, increasing the number of obstacles in the slip plane and making the system harder, corresponding to Stage II in Fig. 1. As the applied stress increases further in Fig. 3(c), there are well-defined regions with essentially constant deformation (low dislocation density, i.e., cells) separated by regions in which there is a sharp change in deformation corresponding to high dislocation densities (i.e., walls). The microstructure in Fig. 3(c) was calculated at a stress corresponding to the maximum in the dislocation density variance that marks the beginning of Stage III in Fig. 1.

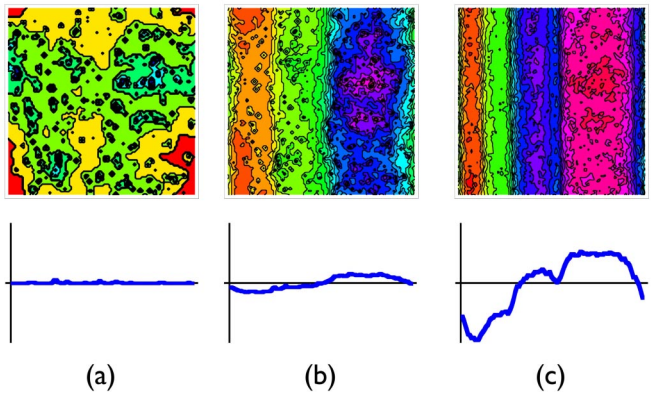

FIG. 3 (color online). Deformation structure during plastic straining. The top set of figures are contour plots of the amount of deformation in units of the Burgers vector (the phase field) during loading. The bottom figures show the value of the deformation on a horizontal line at the center of the simulation cell and are at the same scale relative to each other and plotted around their average values. Dislocation densities correspond to gradients in the deformation. Figures (a)–(c) correspond to applied shear stress $\tau = 0.09 \times 10^{-3}\mu$, $0.25 \times 10^{-3}\mu$, $1.50 \times 10^{-3}\mu$, respectively.

The size distribution of dislocation cells is found experimentally to be fractal [7] with a probability of having a cell of size A being given by

$$n(A) = CA^{-D}, \tag{6}$$

where D is the fractal exponent and $D' = D - 1$ is the fractal dimension. The fractal dimension in the experiments (as in our model) is determined from a two-dimensional slice of material—the 3D fractal dimension is obtained as $D' + 1 = D$. In our simulations, cell interiors are identified as regions where the phase field is constant and, therefore, essentially dislocation free [e.g., Fig. 3(c), bottom]. The fractal dimension for each stress is found by measuring the areas of constant phase field and fitting the resultant distribution to a power law. The fractal dimension is $D \sim 2$ in Stage I and increases with the applied stress, as shown in Fig. 4, up to a value $D \sim 3$. For comparison, the experimental values [7] for copper are also plotted in Fig. 4, and show values similar to the calculations. We note that the experimental methodology for measuring cell size differs from our procedure. In the experimental studies, the walls themselves are counted, ignoring the dislocations in the cell interiors (which are not necessarily resolved in the experiment). We include all dislocations, even those between the well-defined walls seen in Fig. 3(c). However, if the dislocation structures are truly self-similar, as they must be to follow Eq. (6), then the distributions are the same regardless of the scale.

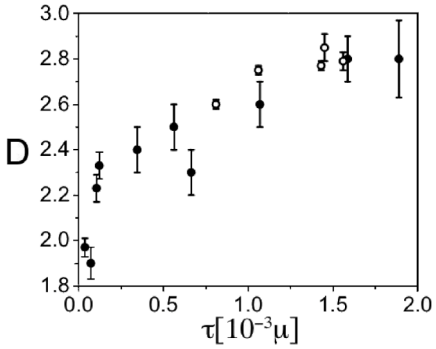

FIG. 4. Fractal dimension D of dislocation cell structures for single crystals deformed at different stresses. Full circles: fractal dimension from phase-field simulations. Open circles: fractal dimension of [100]-oriented Cu single crystals [7].

The two-dimensional picture of deformation developed here enables us to investigate a large range of deformation in single crystals with a single method. We obtain stress-strain behavior that follows experimental trends, showing the presence of different regimes during loading: plastic flow (Stage I), forest hardening (Stage II), and recovery (Stage III). All characteristics of the microstructure, including the relation between dislocation density and stress, the peak in the variance of the density at the Stage II/III transition, and the stress-dependent fractal dimension that characterizes the distribution of cell sizes are in quantitative agreement with what is seen experimentally.

The close correspondence between the model results and experiment has important implications for the interpretation of the deformation of face-centered cubic materials. It has, for example, commonly been accepted that the Stage II to Stage III transition could not happen without enhanced dislocation cross slip [5]. That our model does not include such a mechanism, yet predicts the generally correct behavior, brings that view into question. Rather than increased cross slip, we find simply that the average dislocation density saturates, increased dislocation annihilation occurs, and dislocations rearrange into well-defined cells with a consequent decrease in the hardening rate, i.e., Stage III.

There are, of course, important 3D processes in deformation that are not included in this very simple model. For example, all interactions between dislocations on different slip planes are ignored, except when they cross the planes as ''obstacles.'' Additionally, in a real system, the dislocations in each slip plane also serve as obstacles for dislocations on other planes; i.e., the system is highly coupled. One ramification of this coupling is that walls will coalesce into 3D structures instead of the linear structures seen in our calculations. A fully three-dimensional, self-consistent calculation would be needed to examine that behavior. Despite all of these approximations, however, the net behavior of the model seems valid.

We want to thank Dr. M. Zaiser and Dr. A. Strachan for useful discussions. The work of M. Koslowski and R. LeSar was performed under the auspices of the United States Department of Energy (US DOE under Contract No. W-7405-ENG-36) and was supported by the Division of Materials Science of the Office of Basic Energy Sciences of the Office of Science of the US DOE. M. K. thanks the Computational Materials Science Network of the US DOE/OS/OBES/DMS for their support.

*Electronic address: marisol@lanl.gov.

[1] J. Weertman and J. R. Weertman, in *Physical Metallurgy*, edited by R. W. Cahn and P. Haasen (North Holland, Amsterdam, 1983), Vol. II, pp. 1259–1307.
[2] U. F. Kocks and H. Mecking, Prog. Mater. Sci. **84**, 171 (2003).
[3] A. H. Cottrell, *Dislocations and Plastic Flow in Crystals* (Oxford University Press, Oxford, 1953).
[4] F. R. N. Nabarro, Acta Metall. **37**, 1521 (1989).
[5] A. S. Argon, Scr. Mater. **47**, 683 (2002).
[6] Y. U. Wang, Y. M. Jin, A. M. Cuitiño and A. G. Khachaturyan, Philos. Mag. Lett. **81**, 385 (2001).
[7] P. Hahner, K. Bay, and M. Zaiser, Phys. Rev. Lett. **81**, 2470 (1998).
[8] M. Zaiser, Mater. Sci. Eng. A **309**, 304 (2001).
[9] R. Thomson, M. Koslowski, and R. LeSar, Phys. Lett. A **322**, 207 (2004).
[10] A. H. Cottrell, in *Dislocations in Solids*, edited by F. R. N. Nabarro and M. S. Duesbery (North Holland, Amsterdam, 2002), Vol. 11, pp. vii–xvii.
[11] A. N. Gulluoglu, D. J. Srolovitz, R. LeSar, and P. S. Lomdahl, Scr. Metall. **23**, 1347 (1989).
[12] L. P. Kubin and G. Canova, Scr. Metall. Mater. **27**, 957 (1992).
[13] H. M. Zbib, T. D. de la Rubia, M. Rhee, and J. P. Hirth, J. Nucl. Mater. **276**, 154 (2000).
[14] N. Ghoniem, S. Tong, and L. Sun, Phys. Rev. B **61**, 913 (2000).
[15] M. Koslowski, A. Cuitiño, and M. Ortiz, J. Mech. Phys. Solids **50**, 2597 (2002).
[16] M. Koslowski, R. LeSar, and R. Thomson, Phys. Rev. Lett. **93**, 125502 (2004).
[17] S. Zapperi, A. Vespignani, and H. Stanley, Nature (London) **388**, 658 (1997).
[18] M. Kardar, Phys. Rep. **301**, 85 (1998).
[19] D. L. Turcotte, Rep. Prog. Phys. **62**, 1377 (1997).
[20] J. P. Sethna, K. Dahmen, and C. Myers, Nature (London) **410**, 242 (2001).
[21] J. C. Baret, D. Vandembroucq, and S. Roux, Phys. Rev. Lett. **89**, 195506 (2002).
[22] F. Szekely, I. Groma, and J. Lendvai, Mater. Sci. Eng. A **324**, 179 (2002).